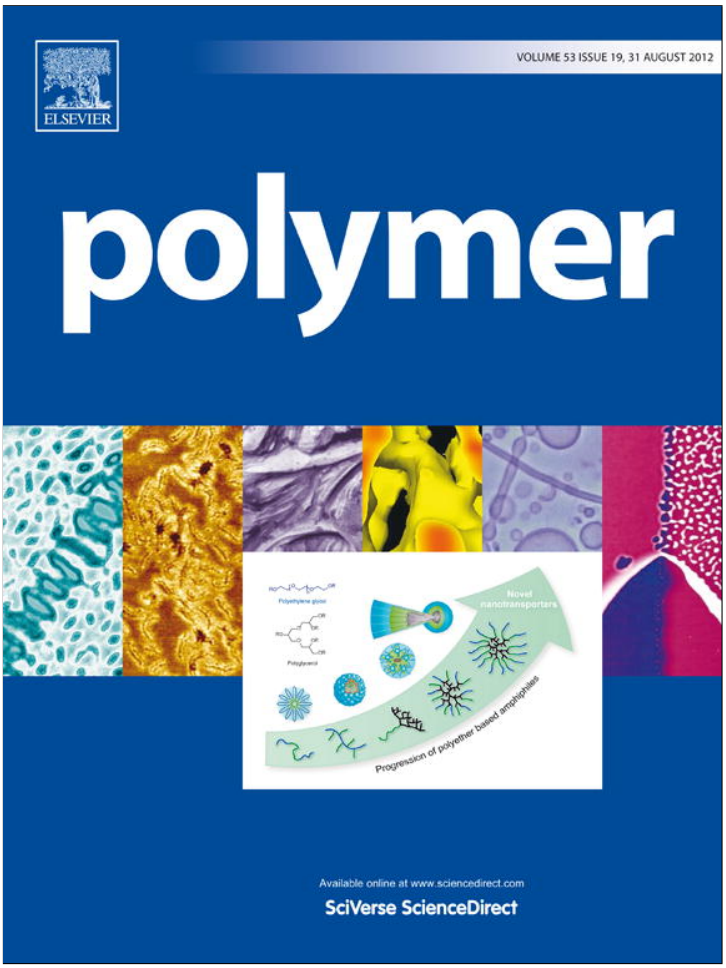

Polymer 53 (2012) 4231–4240

Contents lists available at SciVerse ScienceDirect

Polymer

journal homepage: www.elsevier.com/locate/polymer

Microvascular based self-healing polymeric foam

J.F. Patrick [a,d], N.R. Sottos [b,d,*], S.R. White [c,d]

[a] Department of Civil and Environmental Engineering, University of Illinois at Urbana-Champaign, 205 North Mathews Avenue, Urbana, IL 61801, USA
[b] Department of Materials Science and Engineering, University of Illinois at Urbana-Champaign, 1304 West Green Street, Urbana, IL 61801, USA
[c] Department of Aerospace Engineering, University of Illinois at Urbana-Champaign, 104 South Wright Street, Urbana, IL 61801, USA
[d] Beckman Institute of Advanced Science and Technology, University of Illinois at Urbana-Champaign, 405 North Mathews Avenue, Urbana, IL 61801, USA

ARTICLE INFO

Article history:
Received 1 May 2012
Received in revised form
29 June 2012
Accepted 8 July 2012
Available online 25 July 2012

Keywords:
Self-healing
Microvascular
Polyurethane foam

ABSTRACT

A self-healing microvascular polymeric foam has been developed to improve the resilience of rigid foam core materials for sandwich structures. We investigated the healing of brittle polyisocyanurate (PIR) foam after mode-I crack separation in a 3-point single edge notch bend (SENB) specimen. A two-part healing chemistry based on a commercially available polyurethane (PUR) foam formulation is employed to rebond the interface. Both components are initially sequestered in separate channels in a vascularized SENB geometry. Upon loading and subsequent crack propagation through the network, the healing agents are released and polymerize on contact to create new foam material in the crack plane. An attractive feature of this system is the volumetric expansion of the healing chemistry, demonstrating the ability to repair macro-scale damage. The foaming reaction occurs on the order of minutes at room temperature, enabling rapid in-situ healing. Furthermore, by using a vascular delivery technique, multiple damage–recovery cycles are achieved at consistently high healing efficiencies. Through repeated mechanical testing, we have demonstrated over 100% recovery in fracture toughness for this new class of bioinspired, self-healing cellular materials.

1. Introduction

Natural materials such as bone, wood, sponge, and coral incorporate a variety of life-support functionality within a cellular structure [1,2]. Polymeric foams are synthetic variants employed in engineering applications for their tailorability in microstructure to achieve desired mechanical performance [3,4]. Biomimetic sandwich structures, in which a lightweight core material is bonded between two thin and relatively stiff skins, exhibit high strength-to-weight ratios with appreciable resistance to bending and buckling [5]. Rigid, closed-cell polymeric foams are often utilized as an economical core material in sandwich constructions for aerospace, automotive, civil, marine, and transportation industries [6]. The low density foam core plays a vital role in maintaining structural integrity of the sandwich panel through preservation of face sheet (skin) separation and ensuring adequate load transfer between components.

Numerous failure modes are encountered in sandwich structures that are strongly influenced by the type of loading (static, impact, fatigue), panel geometry, and material constituents [7]. It is not uncommon for one failure event to transition into a subsequent damage mode, rendering the sandwich panel structurally inadequate. Polymeric foam cores often fail in shear, characterized by 45° cracks that initiate at the mid-plane where the shear stress is highest. Under fatigue or overload conditions such as impact, the cracks will then propagate until reaching the face sheets and subsequently change direction to grow along the core-to-skin interface, resulting in core-skin delamination of the sandwich structure [8]. In a recent study conducted on a 3D woven composite-skin and polymer foam-core sandwich panel subjected to highly transient shock wave loading, various core fracture modes were reported in addition to significant, macro-scale core loss [9]. In this manuscript we introduce a viable self-healing solution to macro-scale polymeric foam damage in sandwich panels.

Self-healing strategies for polymers and composites are classified into three main categories: a) intrinsic, b) capsule-based, and c) vascular [10]. Intrinsic systems rely on inherent reversibility of bonding in the polymer matrix and achieve self-healing through mechanisms such as melting of thermoplastic phases, hydrogen bonding, or ionic interactions [11]. Li et al. developed a self-healing syntactic foam consisting of shape memory polymer, glass

* Corresponding author. Department of Materials Science and Engineering, University of Illinois at Urbana-Champaign, 1304 West Green Street, Urbana, IL 61801, USA. Tel.: +1 217 333 1041; fax: +1 217 244 0181.
E-mail address: n-sottos@illinois.edu (N.R. Sottos).

0032-3861/$ – see front matter © 2012 Elsevier Ltd. All rights reserved.
http://dx.doi.org/10.1016/j.polymer.2012.07.021

microspheres, and multi-walled carbon nanotubes incorporated into a composite sandwich panel [12]. Multiple cycles of healing were demonstrated through compression after impact (CAI) evaluation, although the "smart" foam required a thermal-mechanical pre-programming cycle in addition to post-damage heating to 100 °C for 3 h.

In contrast to intrinsic healing, both capsule and vascular-based systems require the containment of liquid healing agents within the polymer matrix that are subsequently released upon damage initiation for self-repair. While most capsule based systems are autonomic, they are inherently limited to small damage volume and a single healing event [13]. Vascular self-healing systems make use of hollow tubes [14,15] or networks of microchannels [16–20] to sequester liquid healing agents throughout the material volume. Many of the successful vascular strategies have relied upon a dual-component approach where released healing agents react upon contact and subsequently polymerize. Thus, healing effectiveness is a function of the liquid components' reactivity and degree of mixing in the damaged region. Recovery in systems relying upon capillary flow and diffusional mixing has been demonstrated over multiple damage–healing cycles in solid polymer materials [16–19]. However, these configurations contained a relatively dense network of interpenetrating capillaries to ensure adequate mixing of components, which can lead to a reduction in mechanical properties [21]. Active delivery (pumping) techniques have been shown to maintain high levels of healing efficiency over multiple healing cycles while reducing the amount of vasculature required [22]. Williams et al. demonstrated recovery in post-impact flexural and compressive strengths for sandwich panels containing pressurized, epoxy resin/hardener filled tubes that were embedded in the foam core to provide healing agent delivery to a debonded core-face sheet interface [23,24].

In this work, we specifically focus on the repair of the cellular core material itself by active delivery of a two-component liquid polyurethane (PUR) foam chemistry. A dual network vasculature is introduced directly into the closed-cell foam, with minimal effect on mechanical properties. Healing performance is evaluated through mode-I fracture by means of a single-edge notched bend (SENB) geometry. In addition to multiple healing cycle capability, we also investigate the effects of channel configuration, delivery volume, component ratio, and reaction kinetics on the healing performance.

2. Materials and methods

2.1. Polymeric foam materials

Two commercial, rigid polyurethane (PUR) foam formulations were employed in this study. Trymer 3000, a PUR modified polyisocyanurate (PIR) produced by DOW Chemical, was obtained from Cook Brothers Insulation, Inc. in the form of 25 mm thick boardstock [25]. X-30, supplied as a two-component liquid PUR system, was obtained directly from TAP Plastics and used as received [26,27]. The first component of the X-30 system, commonly and herein referred to as Part A, contained methylene diphenylene diisocyanate (MDI) [28]. The second component, designated Part B, consisted of a proprietary blend of polyols, hydrofluorocarbon blowing agents, and a chlorinated phosphate ester flame retardant [29].

2.2. Polyurethane foam production

When Parts A and B were combined at a suitable stoichiometry, heat was generated as a result of the polymerization reaction between the diisocyanate and polyol; the resulting temperature increase caused the volatile liquid blowing agents to evaporate and form gas bubbles, which expanded the mixture to produce foam [30]. In order to characterize the expansion properties for the X-30 system, components A and B (6 mL total) were combined at various volumetric ratios and mixed in an open 150 mL beaker at room temperature (RT). After 24 h, the free-rise foam volume was accurately determined by water displacement, since a hydrophobic "skin" was formed on the outer surface of the foam thereby preventing absorption of water. A summary of the expansion results and measured densities for the X-30 and Trymer 3000 systems is provided in Table 1.

Table 1
Comparison of weight related properties for polymeric foams.

Material	Mass density (g/cm^3)	Expansion (vol./vol.)
Trymer 3000 (PIR) foam	0.050 ± 0.001	–
TAP X-30 – Part A	1.22	n/a
TAP X-30 – Part B	1.10	n/a
X-30 (PUR) foam 1.0A:1B[a]	0.055 ± 0.001[b]	20.3 ± 0.3
X-30 (PUR) foam 1.5A:1B	0.073 ± 0.001	15.3 ± 0.2
X-30 (PUR) foam 2.0A:1B	0.091 ± 0.001	12.3 ± 0.2

[a] Mix ratio by volume.
[b] One standard deviation.

2.3. Mechanical evaluation

A three-point single edge notched bend (SENB) mode-I fracture test was selected as the mechanical testing protocol to assess healing performance [31,32]. A schematic representation of the specimen is shown in Fig. 1. Rectangular samples were cut and sanded to dimensions: length (L = 120 mm), height (W = 25 mm), depth (B = 19 mm), whereas the span length (S = 100 mm) was set by the test fixture supports. Prior to testing, a pre-crack (a = 10 mm) was introduced at mid-span on the tensile side of the specimens using a razor blade. Plane-strain fracture toughness, K_{IC}, was calculated according to [33]:

$$K_{IC} = \frac{P_Q}{B\sqrt{W}} f(x), \tag{1}$$

where P_Q is the critical load at fracture and $f(x \equiv a/W)$ is given by,

$$f(x) = \frac{3\frac{S}{W}\sqrt{x}}{2(1+2x)(1-x)^{3/2}} \left[1.99 - x(1-x)\left\{2.15 - 3.93x + 2.7x^2\right\}\right]. \tag{2}$$

The samples were quasi-statically loaded to failure under displacement control at a rate of 25 μm/s. In Fig. 2, typical load versus mid-span displacement data is shown for neat Trymer 3000 PIR and X-30 PUR (1A:1B) cellular materials. The Trymer 3000 exhibited a brittle fracture behavior characteristic of PIR foams and

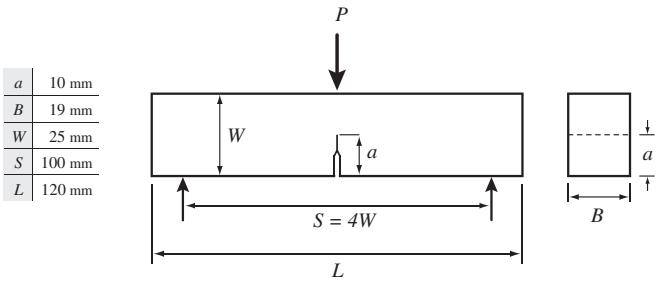

Fig. 1. Schematic of 3-point single edge notched bend (SENB) sample geometry and corresponding dimensions.

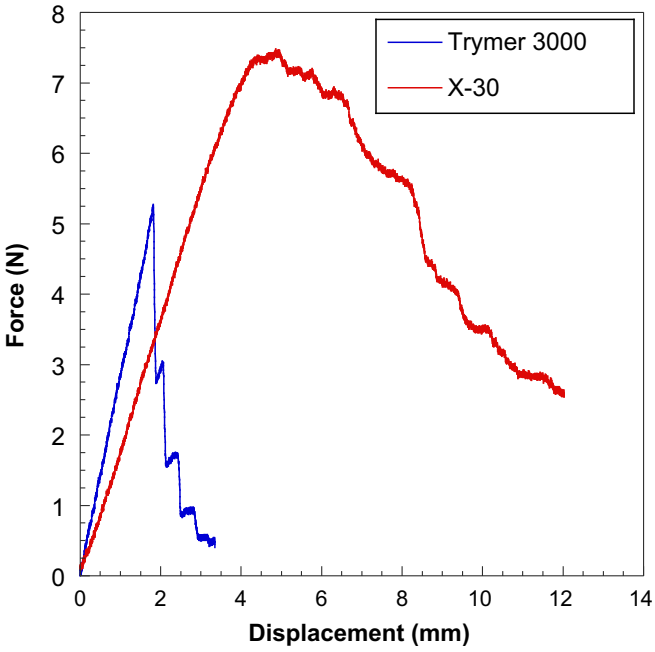

Fig. 2. Representative SENB load-displacement data for brittle fracture (blue) of Trymer 3000 polyisocyanurate (PIR) foam versus ductile tearing (red) behavior of X-30 polyurethane (PUR) foam. (For interpretation of the references to color in this figure legend, the reader is referred to the web version of this article.)

consistent with linear elastic fracture mechanics (LEFM) assumptions, whereas the X-30 displayed a tougher, ductile tearing response more typical of PUR formulations.

2.4. Self-healing sample fabrication

Trymer 3000 is a rigid foam, i.e. closed-cell material (mean diameter 190 ± 80 μm) with low water absorption (<0.7% by vol.), enabling the vascular containment of liquid healing agents within its microstructure [25]. Self-healing SENB specimens of dimensions prescribed in Fig. 1 were vascularized by machining two longitudinal channels with an average diameter of 970 ± 40 μm in both horizontal and vertical configurations, spaced at 5 mm apart, as shown in Fig. 3. Barbed tube fittings were embedded 4.75 mm into both channels, at each end of the sample, and adhesively bonded to the outer cross-sectional face of the foam. These served as sealed connections for the external tubing to supply liquid healing agents. The healing agents, X-30 Parts A and B, were separately contained in plastic syringes connected to the vascular foam samples via tubing, and precisely delivered (± <1%) using a KDS Model 210P syringe pump controlled by computer by means of National Instruments' LabVIEW (v.2009) software.

2.5. Healing test procedure

Fig. 4 summarizes the self-healing test procedure. Initially, each microvascular channel was prefilled with the desired healing component by pumping approximately 2.5 mL of fluid at a volumetric flow rate of 0.5 mL/min and subsequently connecting the open tubing at a wye junction, resulting in a closed system.

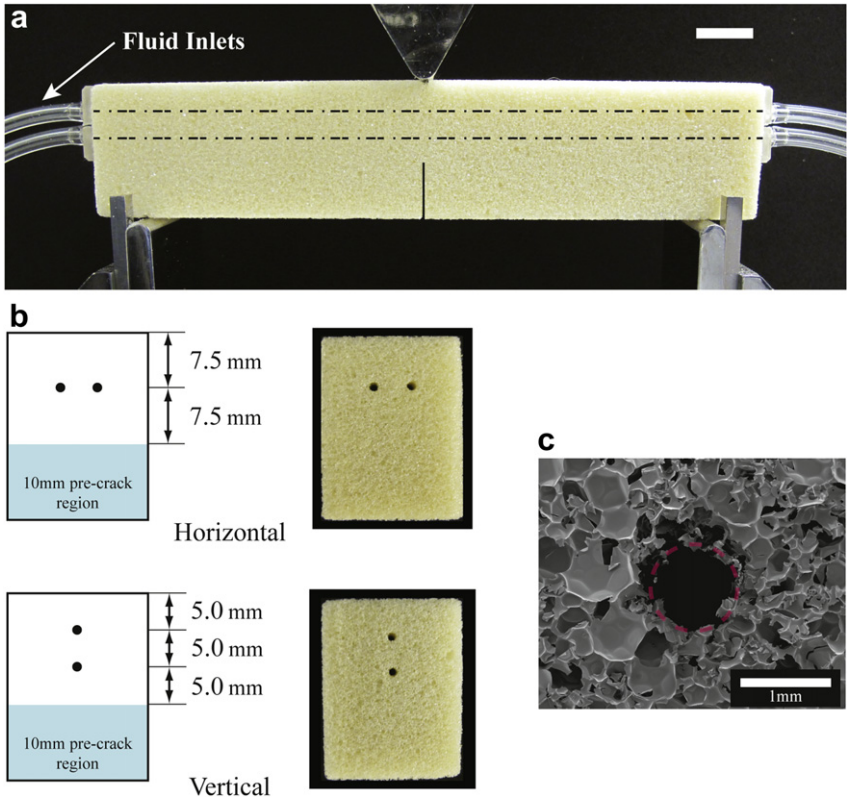

Fig. 3. Self-healing microvascular foam specimens. a) Side view of vascularized Trymer 3000 SENB sample showing tubing connections with vertically oriented channels (indicated by dashed lines) for delivery of healing agents (scale bar = 10 mm); b) Cross-section schematics (left) and optical images (right), of the two channel configurations examined: horizontal (top) and vertical (bottom). [Note: Spacing between channels and average diameter were kept constant at 5 mm and 970 ± 40 μm, respectively]; c) Scanning electron microscope (SEM) image of representative channel topology with color overlay (red) outlining channel perimeter. (For interpretation of the references to color in this figure legend, the reader is referred to the web version of this article.)

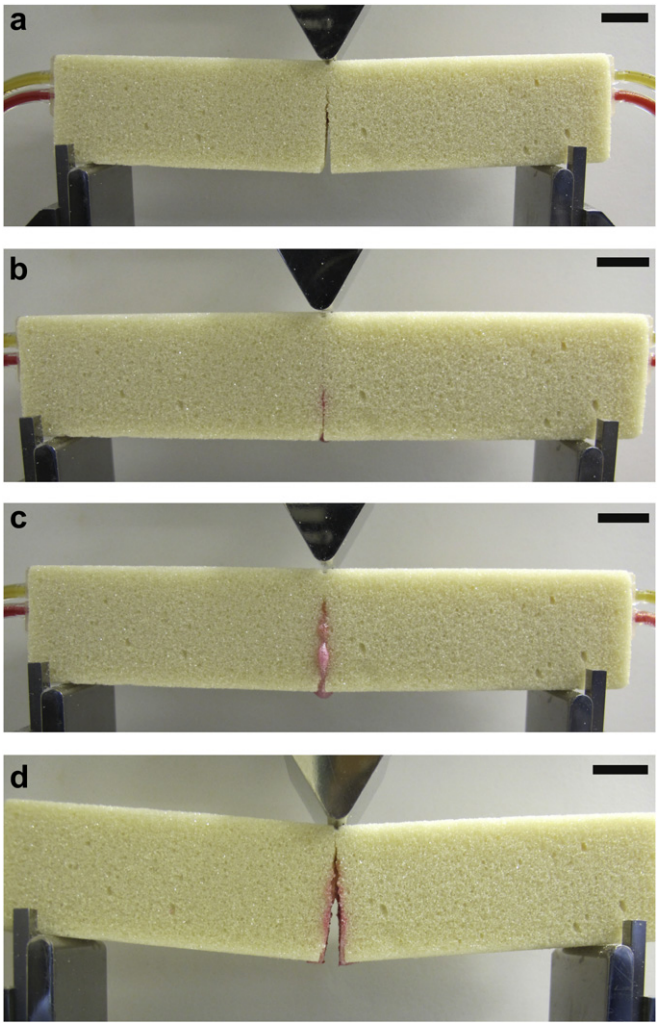

Fig. 4. Self-healing procedure. a) SENB sample with pre-filled channels containing liquid healing agents is loaded (25 μm/s) until fracture propagates through both channels (≈3 mm crosshead displacement) and the loading is paused. One-half of the desired amount of healing agents are delivered to the fracture plane; b) The sample is unloaded (50 μm/s) and concurrently the last half of healing agents are delivered; c) The sample is allowed to heal for a specified time at room temperature (RT ≈ 22 °C); [Not pictured: excess foamed healing material is removed from the outer surfaces and the original pre-crack is reintroduced]; d) The "healed" sample is reloaded (25 μm/s) to failure (scale bars = 10 mm).

Once the channel filling process was complete, the "virgin" self-healing SENB sample was loaded at 25 μm/s to a crosshead displacement of 3 mm to propagate the initial crack and fracture through both channels. The loading sequence was then paused, and one-half of the desired amount of both healing agents was delivered to the crack plane over a time period of 60 s. The sample was then unloaded at 50 μm/s while the remaining half portion of healing agents was concurrently delivered to the fracture plane. The unloaded specimen remained undisturbed on the support fixture for 30 min while the healing (foaming) reaction occurred. After this time, the sample was carefully moved to a fume hood, where it was placed on a mimic support structure and allowed to heal for a prescribed time at room temperature (RT ≈ 22 °C) and 50% relative humidity (RH). Before the "healed" sample was reloaded, excess foamed material was removed from the outer surfaces and the original 10 mm pre-crack length was reintroduced using the same razor blade employed for fracture initiation in the virgin specimen. Ensuring the healed pre-crack length was equivalent to the original pre-crack was vital to calculate accurate healing efficiencies [34].

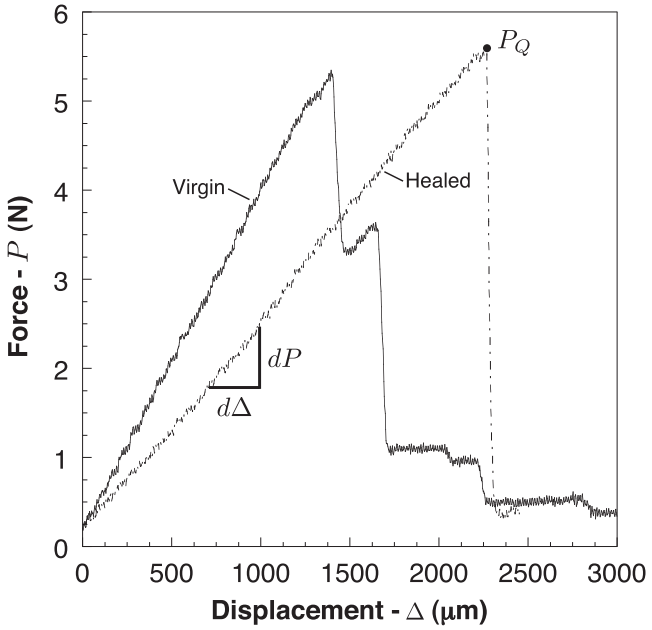

Fig. 5. Representative load-displacement data for virgin fracture (solid) and healed (dashed) tests. The two quantities used to assess healing efficiency are indicated: a) $dP/d\Delta$, i.e. stiffness and b) P_Q, critical failure load for calculating fracture toughness K_{IC}.

Representative load versus mid-span displacement curves for a virgin and healed test are provided in Fig. 5. The virgin curve indicates propagation of the pre-crack first occurred around 1500 μm displacement followed by a series of progressive fractures until the load carrying capacity was virtually nonexistent around 3000 μm displacement. The healed test often indicated a single crack propagation event at failure. The representative healing curve shows a considerable recovery of mechanical integrity both in terms of stiffness ($dP/d\Delta$) and peak load (P_Q), which was used to determine fracture toughness. Correspondingly, two metrics for quantifying healing efficiencies were defined based on stiffness and fracture toughness [35] recovery:

$$\psi \equiv \frac{\frac{dP^{\text{Healed}}}{d\Delta}}{\frac{dP^{\text{Virgin}}}{d\Delta}}, \quad \eta \equiv \frac{K_{IC}^{\text{Healed}}}{K_{IC}^{\text{Virgin}}}. \tag{3}$$

Additionally two "specific" healing efficiencies were calculated to account for the increased weight due to the relatively high-density healing agents sequestered in a lightweight host material:

$$\overline{\psi} \equiv \psi \cdot \left(\frac{\rho^{\text{Virgin}}}{\rho^{\text{Healed}}}\right), \quad \overline{\eta} \equiv \eta \cdot \left(\frac{\rho^{\text{Virgin}}}{\rho^{\text{Healed}}}\right). \tag{4}$$

here density of the virgin material was measured with empty channels, whereas the healed density reflects both liquid filled channels and additional post-healing "foamed" material.

Table 2
Comparison of mechanical properties for neat and vascularized Trymer 3000 PIR foam.

Configuration	Stiffness – $dP/d\Delta$ (N/mm)	Fracture toughness – K_{IC} (MPa. $m^{1/2}$)
Neat	3.48 ± 0.06[a] (1.00)[b]	0.020 ± 0.0003 (1.00)
Horizontal	3.09 ± 0.04 (0.89)	0.018 ± 0.0005 (0.91)
Vertical	3.42 ± 0.09 (0.98)	0.019 ± 0.0005 (0.97)

[a] One standard deviation.
[b] Normalized by neat value.

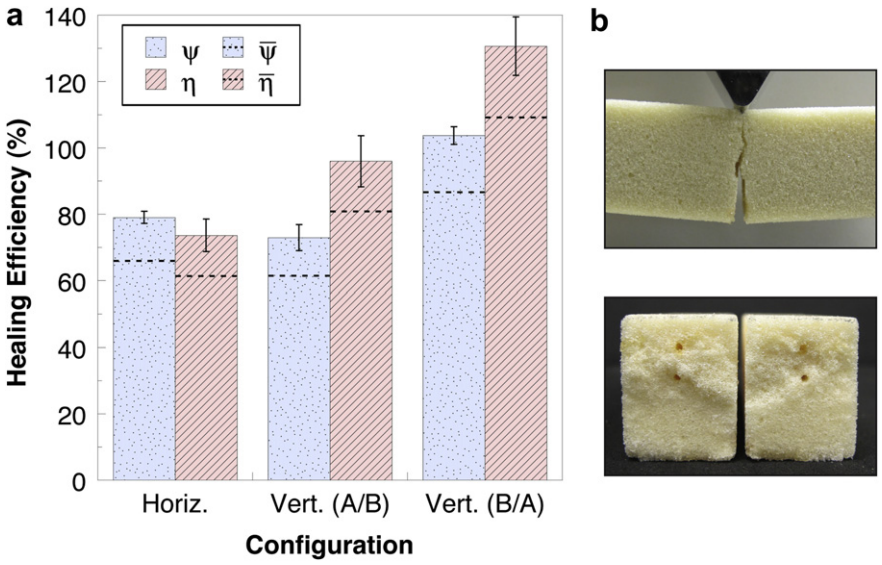

Fig. 6. Effect of channel configuration. a) Plot of healing efficiencies for three configurations investigated: 1) horizontal 2) vertical (A/B) where Parts A and B were contained in the top and bottom channels respectively 3) vertical (B/A) where Parts B and A were contained in the top and bottom channels respectively. 20 μL of each component was delivered at a ratio of 1:1 (by vol.) and tested after 24 h at room temperature. [Note: Vertical error bars represent the standard error from five samples tested]; b) Elevation (top) and cross-section (bottom) images of a healed vertical (A/B) sample exhibiting typical crack deviation around the tougher, healed foam and showing both channels remain clear after post-healing fracture.

3. Results and discussion

3.1. Effect of channel inclusions on mechanical properties

Two types of channel designs were investigated in this study, a horizontal and vertical geometry, as depicted in Fig. 3. To determine the effect of these channel configurations on the structural integrity of the Trymer 3000 PIR foam, a series of SENB tests were carried out. Table 2 summarizes the results of these tests, where 5 specimens for each channel arrangement and a solid or "neat" configuration were evaluated. There was a small reduction in mechanical integrity both in terms of stiffness and fracture toughness for each of the channel designs in comparison to the neat sample. The decrement in the horizontal configuration was 11 and 9% for stiffness and fracture toughness respectively, while the drop-offs for the vertical configuration were substantially lower at 2 and 3%; a reasonable trade-off for acquisition of self-healing functionality.

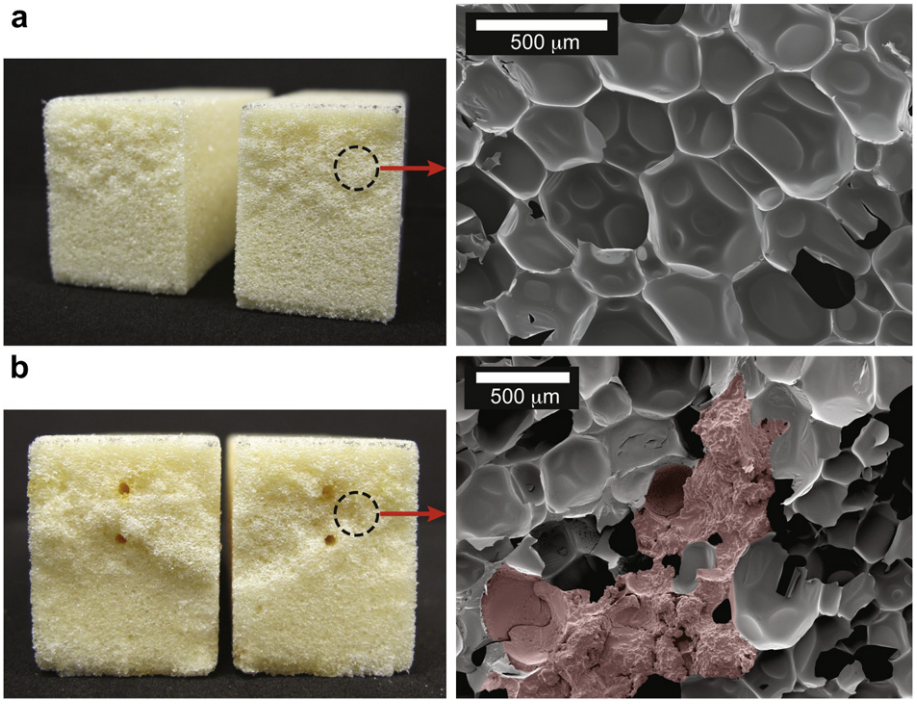

Fig. 7. Fracture surface observations. a) Optical (left) and SEM (right) images of the fracture plane in a neat Trymer 3000 PIR foam; b) Optical (left) and SEM (right) images of a healed PIR foam by microvascular delivery of two-part X-30 PUR foaming agents. False colored red overlay in SEM image outlines healed PUR material surrounded by ruptured PIR foam as a result of post-heal fracture. (For interpretation of the references to color in this figure legend, the reader is referred to the web version of this article.)

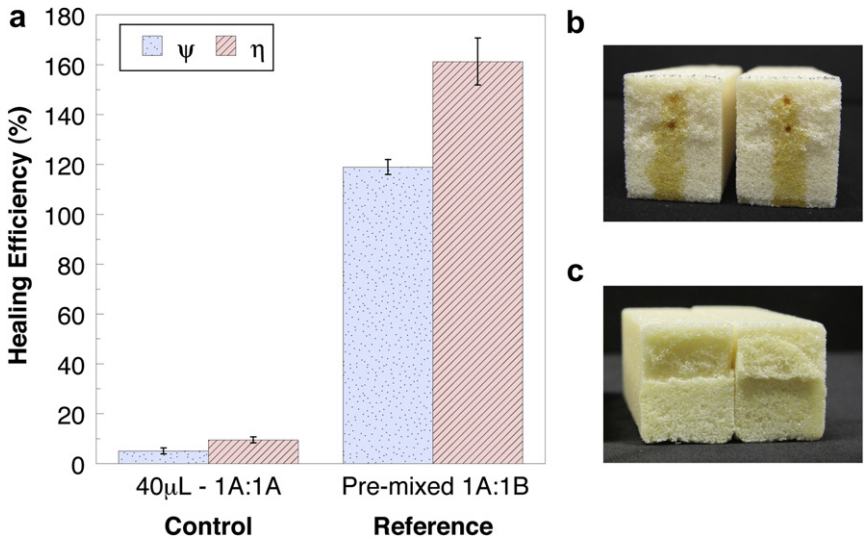

Fig. 8. Control and reference tests. a) Plot of healing efficiencies for vertical control samples where 40 μL of Part A were delivered at a ratio of 1A:1A (by vol.) and reference samples where pre-mixed healing agent at 1A:1B (by vol.) was manually applied to the crack plane. Both sample types were tested after 24 h at room temperature. [Note: Vertical error bars represent the standard error from five samples tested]; b) Cross-section of control sample showing no indication of foamed healing material; c) Cross-section of healed reference sample showing substantial crack deviation around the tougher, healed foam.

3.2. *Effect of channel configuration on self-healing*

The healing performance of both horizontal and vertical channel designs was assessed by delivery of X-30 healing agents for three configurations: 1) horizontal channels containing X-30 Parts A and B, 2) vertical layout (A/B) containing Part A in the upper channel and Part B in the lower channel, and 3) vertical layout (B/A) containing Part B in the upper channel and Part A in the lower channel. For each of these configurations, 20 μL of each healing agent was delivered according to the procedure outlined in Section 2.5 at a volumetric ratio of 1A:1B and retested after 24 h. The healing efficiencies calculated according to Eq. (3) from 5 samples tested are plotted in Fig. 6, together with their specific counterparts as indicated by horizontal dashed black lines drawn across each of the corresponding column plots.

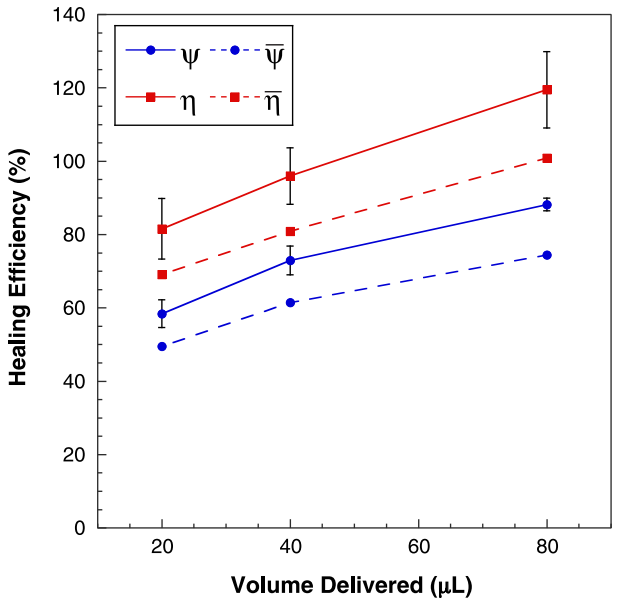

Fig. 9. Effect of volume of healing agent on healing performance. All tests were performed on SENB samples with vertical channel (A/B) configuration at a ratio of 1A:1B (by vol.) and tested after 24 h of healing at room temperature. [Note: Vertical error bars represent the standard error from five samples tested].

Excellent recovery in properties was achieved in all three cases. For the vertical (B/A) configuration, over 100% healing was realized in both standard and specific measures of fracture toughness. The healed crack path (Fig. 6b) often deviated from the initial trajectory followed in the virgin test as a result of the tougher, healed material obstructing the fracture plane. Except for the horizontal configuration, stiffness recovery was lower than fracture toughness recovery. This observation is attributed to the inherent material properties of the PUR foam healing system (Fig. 2), where X-30 exhibits a more ductile (tougher) fracture response at the expense of having lower stiffness in comparison to the Trymer 3000 PIR.

Post-healing evaluation revealed that all of the samples tested for the horizontal and vertical (B/A) configurations resulted in blocked channels where the X-30 Part A (MDI) component was contained. We hypothesize the obstructions are a consequence of the differences in the healing agent wetting characteristics where Part B exhibited a higher degree of foam surface dispersion resulting in undesirable cross-contamination and subsequent polymerization at the channel orifices containing Part A. In contrast, channels remained clear in 80% of the Vertical (A/B) samples, and thus this configuration was used for all subsequent healing tests.

Fig. 7 is a set of optical and scanning electron microscope (SEM) images of fractured surfaces for representative neat and healed samples, illustrating the differences in morphology. The lower 10 mm pre-cracked region is macroscopically “smooth” in both cases, whereas the fractured surfaces exhibit distinct topological features. The neat sample shows a uniform distribution of ruptured cells, while the self-healing surface is characterized by more discrete regions of healed material and a tortuous crack path through the native PIR foam.

Table 3
Syringe combinations used to obtain various healing component ratios.

Component ratio (by vol.)	Syringe A (diameter)	Syringe B (diameter)	Amount delivered
1.0A:1B	5cc (11.99 mm)	5cc (11.99 mm)	20 μL A:20 μL B
1.5A:1B	10cc (14.48 mm)	5cc (11.99 mm)	24 μL A:16 μL B
2.0A:1B	5cc (11.99 mm)	3cc (8.59 mm)	27 μL A:13 μL B

3.3. Controls and reference tests

Five control specimens containing solely Part A in both vertical channels were evaluated by delivering a total of 40 μL at a ratio of 1A:1A to the crack plane and tested after 24 h at room temperature (RT) and 50% relative humidity (RH). Additionally, a set of "reference" experiments were conducted to establish an upper bound on healing efficiency. These reference tests consisted of ten, neat Trymer 3000 SENB specimens fractured in two and subsequently healed by applying pre-mixed X-30 components at a ratio of 1A:1B directly to each fracture surface. The two halves were placed back in contact and mechanically constrained in order to prevent the expansive foam from pushing the specimens apart.

The results of these two experiments are summarized in Fig. 8a. The control samples show no appreciable healing. The efficiencies reported are due to the presence of remaining ligament of intact material after the initial (virgin) test. Fig. 8b is an optical image of the cross-section of a control sample after healing showing no evidence of foamed healing material on the fracture plane. In contrast, the reference samples display a substantial amount of mechanical recovery, 120% and 160% in terms of stiffness and fracture toughness recovery, respectively. Importantly, over 100% stiffness recovery was attained, despite the fact that the X-30 PUR foam inherently has a lower modulus than the Trymer 3000 PIR material. This effect can be attributed to the high degree of densification for the pre-mixed X-30 foam as it attempts to expand inside the crack plane under applied mechanical confinement [1,30].

3.4. Delivery amount and component ratio

Healing performance was influenced by the total volume of healing agent delivered and the ratio of the components. Fig. 9 summarizes the results obtained from five samples at three total volumes (20, 40, 80 μL) of healing agents delivered at a ratio of 1A:1B through the vertical (A/B) configuration and tested after 24 h at RT. The plot indicates a nearly linear increase in both stiffness and fracture toughness healing efficiencies with increasing healing agent delivered to the crack plane. As the amount of healing agents delivered increases, more PUR foam is produced to expand and fill a greater portion of the fractured region, thus leading to higher healing efficiencies. However, a noticeable amount of post-heal bending deformation (positive curvature) was produced in the 80 μL specimen as a result of foamed healing material expanding the crack faces.

A series of experiments in which the ratio of components varied was conducted by holding the total healing agent amount at 40 μL and varying the delivered volumetric proportions of X-30 Parts A to B. Altering the volumetric ratios was accomplished by using syringes of different diameters (Table 3) at a prescribed delivery rate. Five samples for each ratio of 1.0A:1B, 1.5A:1B, and 2.0A:1B were investigated for the vertical (A/B) configuration, and healing was evaluated after 24 h at RT. The results, summarized in Fig. 10, show a nearly linear increase in both healing efficiencies with increasing proportion of Part A. Increasing the Part A content produced a denser foam (Table 1), which has been widely reported to improve mechanical properties [1,5].

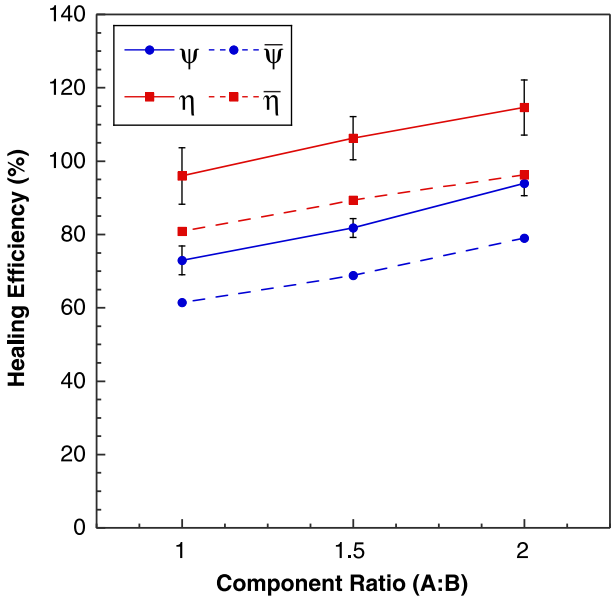

Fig. 10. Effect of healing component ratio on healing performance. All tests were performed on SENB samples with vertical channel (A/B) configuration at a total delivery amount of 40 μL and tested after 24 h of healing at room temperature. [Note: Vertical error bars represent the standard error from five samples tested].

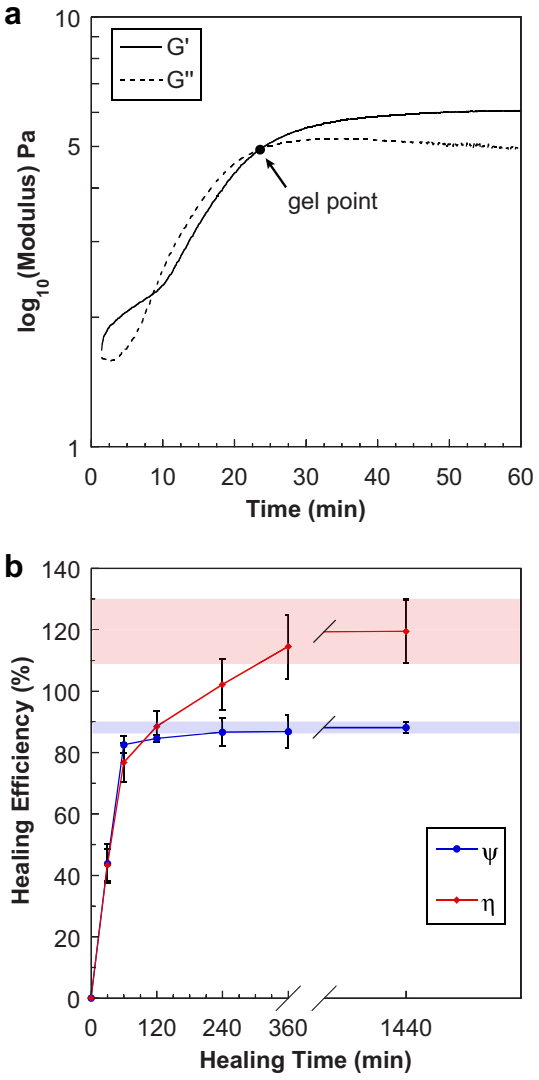

Fig. 11. Healing kinetics. a) Rheometric data (parallel plates) for X-30 PUR foam cured at room temperature [plate diameter = 25 mm; Oscillatory shear parameters: amplitude = 0.0012 rad, frequency = 10 rad/s]; b) Plot of healing efficiencies as a function of healing time at room temperature for 80 μL of healing agents delivered through vertical channels (A/B) at a constant ratio of 1A:1B (by vol.). [Note: Vertical error bars represent the standard error from five samples tested].

On average, the specific healing efficiencies were 19 percent lower than the standard metrics, strictly due to increased weight from the sequestered liquid healing agents. The theoretical weight addition can be estimated by calculating the volume of healing agent inside a smooth, cylindrical channel (120 mm long, average diameter 970 μm) to be 0.09 mL, and then multiplying by the measured densities (Table 1) of X-30 Parts A and B. Based on these assumptions, a dual-channel SENB sample should only experience a relative weight penalty of 7%. However, even closed-celled PIR materials experience some liquid absorption (Trymer 3000: <0.7% by vol.), which may be further increased on the interior channel walls due to rupture of the cells during the machining process. The actual, measured volume of healing agent inside a channel was on average 0.22 ± 0.02 mL, more than double the theoretical value assuming a nonporous channel profile. Using these results, the calculated weight penalty of 18 ± 1.3% correlates closely with the average measured weight increase of 19%. Hence, it is essential to consider the absorption properties of the cellular host material in order to minimize the weight penalty incurred from vascular containment of liquid healing agents.

3.5. Healing kinetics

The reaction between X-30 Parts A and B is rapid, even in the absence of complete mixing, with PUR foam ejecting from the crack plane on the order of minutes. The reaction kinetics were characterized following the procedure reported by Nabata et al. [36] in which parallel plate rheometry (TA Instruments AR-G2) was performed on pre-mixed X-30 (1A:1B) to determine the degree of polymerization as a function of time. Fig. 11a is a plot of the evolution of the measured storage (G') and loss moduli (G'') versus cure time. After 24 min, the storage modulus surpasses the loss values, indicating that gelation has occurred. The stiffness at this point has reached 81% of the plateau value attained in 60 min, demonstrating the rapid reaction kinetics associated with these PUR foam systems even at room temperature.

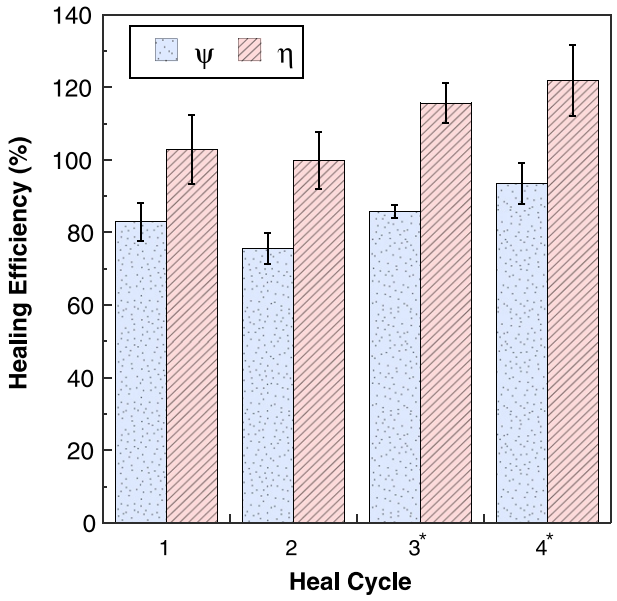

Fig. 12. Multiple healing cycles. Healing efficiencies are plotted for each cycle of healing. SENB samples with vertical channel (A/B) configuration were used with a pumping ratio of 1A:1B and tested after 24 h of healing at room temperature. The total amount of healing agent delivered in cycles 3* and 4* was 160 μL compared to 80 μL delivered in each of the first two cycles. [Note: Vertical error bars represent the standard error from five samples tested].

The effect of healing time on healing performance was investigated by testing 5 samples after increasingly longer periods of time at room temperature (30 min, 1 h, 2 h, 4 h, 6 h, 24 h). In all cases the total amount of healing agent was held constant at 80 μL at a constant pumping ratio of 1A:1B. The results of these experiments are shown in Fig. 11b. After only 30 min, healing efficiencies had reached approximately 43%. After 60 min, stiffness recovery had reached 83% and thereafter increased slowly to a maximum of 88% after 24 h. Recovery of fracture toughness occurred more slowly although nearly full performance was achieved after 6 h healing time. Interestingly, both stiffness and fracture toughness healing efficiencies after 24 h had reached an equivalent 74% of the maximum values established by the reference tests, demonstrating the effectiveness of vascular delivery and resulting in-situ mixing.

3.6. Multiple healing cycles

One advantage of microvascular self-healing systems over prior capsule based approaches is the ability to achieve multiple healing cycles through continued delivery of liquid healing agents.

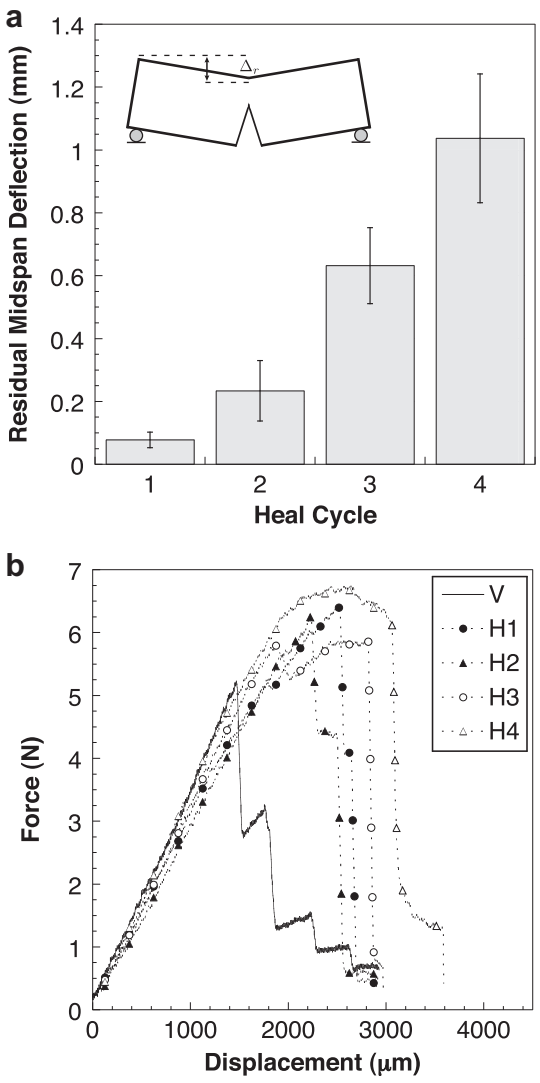

Fig. 13. Mechanical behavior for multiple healing cycles. a) Plot of residual midspan displacement measured after each corresponding heal cycle. [Note: Vertical error bars represent the standard error from five samples tested]; b) Representative load versus midspan displacement data for virgin (V) and successive 24 h heal cycles (H1, H2, H3, H4).

Maintaining clear channels is absolutely critical to achieving repeated healing. The vertical (A/B) channel configuration was selected for this portion of the study, since this design showed less propensity for channel blockage after a single healing event. Fig. 12 summarizes the results obtained from five samples subjected to repeated fracture and healing events separated by 24 h intervals at room temperature. In both the first and second cycles a total of 80 μL (1A:1B) of X-30 liquid PUR constituents were delivered to the crack plane, whereas in each of the third and fourth cycles that amount was doubled to 160 μL (1A:1B) due to a rougher fracture surface inhibiting dispersion of the healing agents into the fracture plane.

Remarkably, not only are multiple healing cycles achieved, but high healing efficiencies (>100%) are maintained provided the vasculature remains clear. After four cycles of healing (in all samples) however, the top channel containing Part A (MDI) became obstructed by healed foam material thereby preventing subsequent healing events. The accumulation of healed material in the fracture plane also had an impact on the shape recovery of the SENB samples. Fig. 13a is a plot showing the increase in residual or irrecoverable midspan deflection, Δ_r, along the vertical load line with successive healing cycles. After the first two cycles, the amount of residual deformation remained less than 10% of the total deflection ($\approx$3000 μm) applied to the midspan of the SENB sample during the loading sequence. However after the second and third cycles, the percentages had exceeded 20 and 30% respectively. A considerable portion of the residual deformation is attributed to the accrual of healed material on the fractured surfaces, thereby preventing full closure of the crack upon elastic unloading. Additionally, as the tougher "healed" PUR foam material occupies a greater portion of the damage zone, the failure behavior begins to transition from linear elastic brittle fracture to a plastic ductile tearing response characteristic of the X-30 system (Fig. 2). This irrecoverable deformation from tearing is observed in the representative multiple cycle load versus midspan displacement data in Fig. 13b. The induced plasticity becomes significant for heal cycles 3 and 4.

4. Conclusions

Self-healing polymeric foam was achieved by microvascular fluid delivery of a two-part, commercially available polyurethane (PUR) foam formulation. Vascular, single edge notched bend (SENB) specimens were designed, fabricated, and tested in mode-I fracture to assess mechanical recovery. Healing efficiencies exceeding 100% were realized through proper selection of the material system and optimization of delivery parameters. The rapid, expansive nature of the PUR foam reaction provided for fast healing kinetics, with over 75% recovery in both stiffness and fracture toughness in 1 h at room temperature. Additionally, multiple damage–healing cycles were attained without sacrifice to healing efficiency or structural integrity. The commercial availability of materials used in addition to the straightforward fabrication techniques employed provide a feasible self-healing concept for sandwich panels, thereby mitigating costly service demands and alleviating safety concerns over hidden damage.

Acknowledgments

The authors would like to acknowledge funding provided by the Department of Homeland Security (Award # 2008-ST-061-ED0001). In addition, the authors would like to thank members of the Autonomous Materials Systems group at the University of Illinois at Urbana-Champaign: D.J. Fairfield, Dr. Andrew Hamilton, Amanda Jones, Dr. Cassandra Kingsbury, Brett Krull, Dr. Chris Mangun, and Dr. David McIlroy. Finally, thanks to Dustin Burns, Greg Milner, and Darold Marrow of the Aerospace and Civil Engineering machine shops for assistance with test fixture modifications and sample fabrication.

References

[1] Ashby M. The mechanical properties of cellular solids. Metallurigcal Transactions A 1983;14A:1755–69.
[2] Gibson L, Ashby M, Harley B. Cellular materials in nature and medicine. Oxford, UK: Cambridge University Press; 2010.
[3] Maiti S, Ashby M, Gibson L. Fracture toughness of brittle cellular solids. Scripta Metallurgica 1984;18:213–7.
[4] Lee S, Ramesh N. Polymeric foams: mechanisms and materials. Boca Raton, FL, USA: CRC Press; 2004.
[5] Gibson L, Ashby M. Cellular solids: structure and properties. 2nd ed. Oxford, UK: Cambridge University Press; 1997.
[6] Zenkert D, Burman M. Tension, compression and shear fatigue of a closed cell polymer foam. Composites Science and Technology 2009;69(6):785–92.
[7] Allen H. Analysis and design of structural sandwich panels. Oxford, UK: Pergamon Press; 1969.
[8] Zenkert D, Vikstrom M. Shear cracks in foam core sandwich panels: nondestructive testing and damage assessment. Journal of Composites Technology & Research 1992;14:95–103.
[9] Tekalur S, Bogdanovich A, Shukla A. Shock loading response of sandwich panels with 3-d woven e-glass composite skins and stitched foam core. Composites Science and Technology 2009;69:736–53.
[10] Blaiszik B, Kramer S, Olugebefola S, Moore J, Sottos N, White S. Self-healing polymers and composites. Annual Review of Materials Research 2010;40:179–211.
[11] White S, Blaiszik B, Kramer S, Olugebefola S, Moore J, Sottos N. Self-healing polymers and composites. American Scientist 2011;99:392–9.
[12] Li G, John M. A self-healing smart syntactic foam under multiple impacts. Composites Science and Technology 2008;68:3337–43.
[13] White S, Sottos N, Geubelle P, Moore J, Kessler M, Sriram S, et al. Autonomic healing of polymer composites. Nature 2001;409:794–7.
[14] Pang J, Bond I. A hollow fibre reinforced polymer composite encompassing self-healing and enhanced damage visibility. Composites Science and Technology 2005;65:1791–9.
[15] Trask R, Williams G, Bond I. Bioinspired self-healing of advanced composite structures using hollow glass fibres. Journal of the Royal Society Interface 2007;4:363–71.
[16] Toohey K, Sottos N, Lewis J, Moore J, White S. Self-healing materials with microvascular networks. Nature Materials 2007;6:581–5.
[17] Toohey K, Hansen C, Sottos N, Lewis J, White S, Sottos N. Delivery of two-part self-healing chemistry via microvascular networks. Advanced Functional Materials 2009;19:1399–405.
[18] Hansen C, Wu W, Toohey K, Sottos N, White S, Lewis J. Self-healing materials with interpenetrating microvascular networks. Advanced Materials 2009;21:4143–7.
[19] Hamilton A, Sottos N, White S. Self-healing of internal damage in synthetic vascular materials. Advanced Materials 2010;22:5159–63.
[20] Norris C, Meadway G, O'Sullivan M, Bond I, Trask R. Self-healing fibre reinforced composites via a bioinspired vasculature. Advanced Functional Materials 2011;21:3624–33.
[21] Hamilton A, Sottos N, White S. Local strain concentrations in a microvascular network. Experimental Mechanics 2010;50:255–65.
[22] Hamilton A, Sottos N, White S. Pressurized vascular systems for self-healing materials. Journal of the Royal Society Interface 2012;9(70):1020–8.
[23] Williams H, Trask R, Bond I. Self-healing composite sandwich structures. Smart Materials and Structures 2007;16:1198–207.
[24] Williams H, Trask R, Bond I. Self-healing sandwich panels: restoration of compressive strength after impact. Composites Science and Technology 2008;68(15–16):3171–7.
[25] The DOW Chemical Company, P.O. Box 1206, Midland, MI 48641, USA, Product Information: Trymer 3000 polyisocyanurate foam Insulation (March 2007).
[26] TAP Plastics, 6475 Sierra Lane, Dublin, CA 94568, USA, Technical Data: X-30 Expanding Foam (May 2004).
[27] TAP Plastics, 6475 Sierra Lane, Dublin, CA 94568, USA, Product Bulletin: X-30 Polyurethane Foam (April 2004).
[28] TAP Plastics, 6475 Sierra Lane, Dublin, CA 94568, USA, MSDS: TAP X-30 polyurethane foam SIDE A (April 2010).
[29] TAP Plastics, 6475 Sierra Lane, Dublin, CA 94568, USA, MSDS: TAP X-30 polyurethane foam SIDE B (April 2010).
[30] Kapps M, Buschkamp S. The production of rigid polyurethane foam, tech. rep. Bayer Material Science; 2004.
[31] ASTM International. ASTM D5045: standard test methods for plane-strain fracture toughness and strain energy release rate of plastic materials; 2007.
[32] Kabir M, Saha M, Jeelani S. Tensile and fracture behavior of polymer foams. Materials Science and Engineering 2006;A 429(1–2):225–35.

[33] Anderson T. Fracture mechanics: fundamentals and applications. 3rd ed. Boca Raton, FL, USA: CRC Press; 2005.
[34] Brown E. Use of the tapered double-cantilever beam geometry for fracture toughness measurements and its application to the quantification of self-healing. Strain Analysis for Engineering Design 2011;46:167–86.
[35] Brown E, Sottos N, White S. Fracture testing of a self-healing polymer composite. Experimental Mechanics 2002;42:372–9.
[36] Nabata Y, Mamada A, Yamasaki H. Study of the curing process giving the rigid polyurethane foam by dynamic viscoelastic method. Applied Polymer Science 1988;35:155–66.